JOURNAL OF APPLIED ELECTROCHEMISTRY 15 (1985) 293–306

*Determination of state-of-discharge of zinc–silver oxide button cells. I. Galvanostatic measurements**

JEAN-PAUL RANDIN

ASULAB S.A., Passage Max-Meuron 6, 2001 Neuchâtel, Switzerland

Received 1 June 1984; revised 10 July 1984

Galvanostatic measurements have been performed on numerous types of $Zn–Ag_2O$ button cells, including low and high drain versions of multiple sizes with various lot numbers from six manufacturers throughout the world. The aim was to find a fast, reliable, nondestructive state-of-discharge indicator. The passivation time constant, $i\tau^{1/2}$, was found to decrease with increasing state-of-discharge. A linear relationship was usually found between 40 and 100% state-of-discharge. The passivation time was not retained at the preferred state-of-discharge indicator due to the removal of excess charge during the measurement and the long recovery time necessary to return to the characteristics of the cell which prevailed before passivation. The initial passivation time constant increased linearly with increasing capacity or volume of the cell with a slope depending on the manufacturer. The slope or $\Delta E/\Delta t$ value of the potential vs time curve was found to be the more reliable and practical state-of-discharge indicator. Applications are limited to a 'go/no go' test with a selection at 50 ± 10% state-of-discharge. Bell shape changes of the passivation time constant vs state-of-discharge in the 0–40% state-of-discharge range preclude the selection at low state-of-discharge values. The test current giving an appropriate slope between either 2 and 10 s or 10 and 30 s was found to follow the rough correlation: i_{test} (mA) $\simeq$ 0.5 C nominal (mA h). The charge withdrawn during the measurement was about 0.1% of the nominal capacity. A calibration was needed for each cell dimension, each manufacturer and possibly, each lot number to set the precise current level giving the appropriate $\Delta E/\Delta t$ value at 50 ± 10% state-of-discharge. Success ratios of the predictions were in the 90% range with a known calibration. The wrong predictions were mainly due to the large dispersion of the electrical characteristics of the cells and to the low state-of-discharge value which is needed for practical applications.

1. Introduction

There has been a need for a reliable, nondestructive state-of-discharge indicator for many of the most commonly used primary batteries. As proposed by Kornfeil [1] 'state-of-discharge' is used in this paper instead of the more prevalent 'state-of-charge' because the latter may convey the concept of rechargeability. The state-of-discharge of a battery refers to the ratio of (used capacity at a given instant) to (the maximum capacity available from the battery). A knowledge of this parameter predicts the residual capacity and cautions the user about the need for an impending battery replacement.

The method chosen must fulfil several requirements. In particular, it must:

1. be nondestructive
2. not discharge the battery appreciably
3. give a reading independent of cell history
4. require less than one minute for the measurement
5. be operable by an unskilled person

Many attempts have been reported in the literature to determine the state-of-discharge of primary and secondary batteries by measurement of properties such as dissolved-ion concentration, open circuit voltage, closed circuit voltage, internal

* This is the first of a series of papers dedicated to Professor Ernest Yeager on the occasion of his 60th birthday.

0021–891X/85 $03.00 + .12 © 1985 Chapman and Hall Ltd.

resistance, open circuit voltage recovery transient, alternating current phase shift, alternating current impedance and its components. The methods were mainly applied to secondary batteries [2, 3].

We restricted our interest in button size primary cells, mainly Zn–Ag_2O, of the type used in watches, pocket calculators and other low power electronic equipments.

The galvanostatic test method described by Kornfeil [1] for Zn–HgO cells in which the terminal voltage was measured 90 s after the start of a constant discharge current and taken as a measure of the state-of-discharge was found to be too dependent on the internal resistance of the cell and on its change with discharge. The tangent drawn to E–i curves at various constant di/dt [4] or the potential reached at a given current or time on the same E–i curves were not found to give accurate results.

The object of the present study was to identify a suitable, sensitive parameter of the Zn–Ag_2O button cells and develop this into a practical device capable of predicting the residual capacity in cells of unknown storage and discharge history. Ideally, the curve relating the electrical response to the state-of-discharge should be smooth, preferably a straight line. The slope of this curve should be sufficiently large to resolve a difference in the state-of-discharge of 10% with a particular set of experimental parameters. If this goal can not be achieved, a very useful test would be to select cells which have a state-of-discharge $\leqslant 30\%$. A less demanding but still useful criterion would be selection at a threshold of $\leqslant 50\%$ state-of-discharge.

The present paper describes the results obtained with the galvanostatic method. The transition time constant was investigated as a function of the state-of-discharge and the slope of the E vs time curves is proposed as the state-of-discharge indicator. An attempt was also made to correlate the transition time constant and the test current with the nominal capacity of the cells in order to predict the level of current to be used to find an appropriate slope of the E vs t curve for a selection at 30–50% state-of-discharge.

2. Experimental details

Numerous sizes of low and high drain cells from six international manufacturers were investigated (see Table 1). For each type of cell at least 25 samples were used. Four lots of five samples each were discharged to 40, 60, 75 and 90% state-of-discharge, respectively. Five samples were kept undischarged. After the galvanostatic measure-

Table 1. Sizes of the cells investigated from six manufacturers (A–F) with the nominal capacity of each cell in mA h (a) Low drain cells

Height (mm)	*Diameter (mm)*							
	6.8		*7.9*		*9.5*		*11.6*	
1.1	A	7	A	8				
1.4			A	15				
1.6	A	11	A	19	A	24		
	B	11	B	14				
							C	33
			D	20	D	23	D	22
2.1	A	15	A	20	A	30	A	48
	B	18	B	22	B	30	B	50
	C	16	C	20	C	33	C	48
	D	15					D	41
	E	17	E	25	E	38		
	F	16	F	20				
2.6	A	24	A	29	A	52		
			B	30	B	45		
	C	20	C	24	C	40		
					D	55		
			E	32				
3.1			A	37			A	80
							C	72
3.6			A	45			A	100
4.2							A	120
							F	113

(b) High drain cells

Height (mm)	*Diameter (mm)*							
	6.8		*7.9*		*9.5*		*11.6*	
2.1					A	28		
			E	27			F	50
2.6			A	29	A	52		
			C	30	C	40		
					D	55		
			E	32	E	56		
3.1							A	80
							F	95
3.6							A	100
			F	35				
4.2							A	120
5.4			F	75			F	200

ments, the resistive discharges were continued after an equilibration period of at least two days to determine the total capacity of each cell.

The discharges were performed on constant loads at ambient temperature. The resistive load was chosen for each size to have a total discharge time of about 30 days. Current drains varied between 9.7 μA for the smaller size and 167 μA for the larger one. A cut-off voltage of 1.2 V was used.

The internal resistance was determined from the instantaneous voltage drop measured with a storage oscilloscope under a 1500 Ω load.

The galvanostatic measurements were performed with a Tacussel Type Bipad potentiostat used as a galvanostat. The potential–time curves were traced on a X–time recorder. At least 2 days were allowed to elapse for diffusional processes within the cell to become complete between two consecutive experiments. The measurements were carried out at 20 ± 1° C in a constant temperature box. This procedure was necessary since a 10 and 16 mV (° C)$^{-1}$ shift of the potential at a given time around 20° C was observed for some cells at 0 and 66% state-of-discharge, respectively. By contrast, the $\Delta E/\Delta t$ change vs temperature around 20° C was negligibly small.

Some experiments were also performed at 0 and 50° C to determine the activation energy. The measurements were carried out at the three temperatures on the same samples. The cells were equilibrated for a minimum of 1 h at each temperature and a recovery time of at least 2 days was allowed to elapse between each measurements. The temperature cycle was 50, 20, 0 and 20° C. The samples were measured twice at 20° C to check the reproducibility.

The potential drop at the transition time was not always sharply defined. Under these conditions, the criterion used to define the termination of useful discharge was the attainment of a potential 0.3 V below the potential reached after 5 s. The time when this occurred was defined as τ and assumed to correspond to the time of polarization required to cause passivation.

The working geometrical area is defined by the zinc anode. It does not necessarily correspond to the internal diameter of the case and changes from one manufacturer to the other depending on the internal construction. For manufacturer A, the electrode geometrical area was as follows:

diameter (mm)	6.8	7.9	9.5	11.6
area (cm^2)	0.13	0.16	0.27	0.48

A few experiments were performed using a Hg/HgO (1N NaOH) reference electrode introduced into a hole drilled through the positive case as described in Part III of this series [5].

Except for the experiments involving the variation of the temperature and the use of a reference electrode, the measurements were performed on all the types of cells shown in Table 1. Only typical behaviour will be reported in the present paper to illustrate the technique.

3. Results

Typical galvanostatic curves for five low drain cells of the same lot, at several states-of-discharge, are shown in Fig. 1. The value of the current level was selected to have a transition time of about 100 to 200 s for the undischarged cell. The transition time decreased with the state-of-discharge, at least for a state-of-discharge larger than 40%. The same trend was observed for high drain cells (Fig. 2). For the latter cells the drop of potential at the transition time was usually sharper than for low drain cells. Sharper or more gradual curves than those shown in Figs. 1 and 2 have also been found.

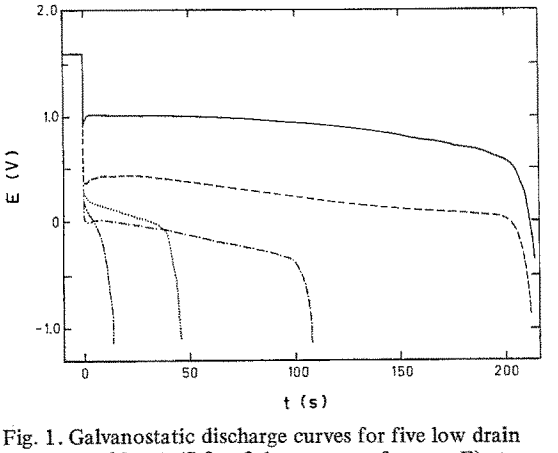

Fig. 1. Galvanostatic discharge curves for five low drain cells at i = 25 mA (7.9 × 2.1 mm, manufacturer E) at (0) (———), 40 (– – – –), 57 (–·–·–), 73 (·····) and 88% state-of-discharge (–··–··–··–).

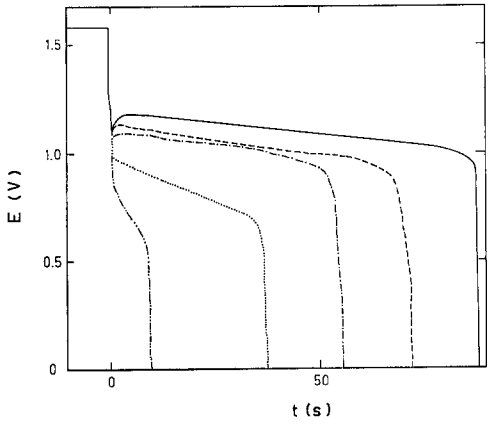

Fig. 2. Galvanostatic discharge curves for five high drain cells at $i = 42$ mA (7.9 X 2.1 mm, manufacturer E) at 5 (———), 40 (– – – –), 60 (–·–·–), 75 (·····) and 90% state-of-discharge (–··–··–··–).

The galvanostatic discharge curves with respect to a reference electrode introduced in a hole drilled through the positive (Ag_2O) terminal show that the polarizations at the beginning of the discharge are due to both electrodes while at the end the diffusion limitation occurs entirely at the zinc electrode (Fig. 3). The transition time measured at the cell terminals is therefore characteristic of the passivation occurring at the zinc electrode. This passivation is associated with a diffusion-controlled zincate ion saturation or supersaturation of the solution layer adjacent to the electrode resulting in the deposition of zinc oxide.

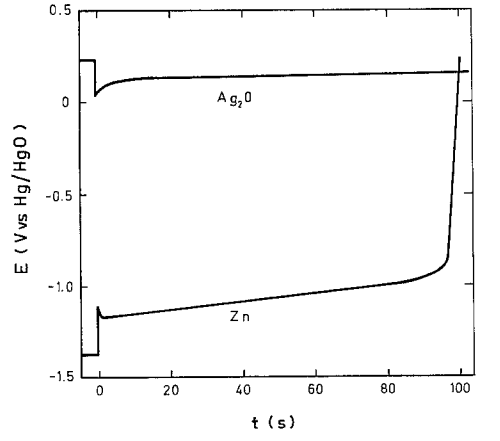

Fig. 3. Galvanostatic discharge curves of the zinc and silver oxide electrodes vs Hg/HgO reference electrode at $i = 40$ mA in an undischarged, high drain cell (7.9 X 2.1 mm, manufacturer E).

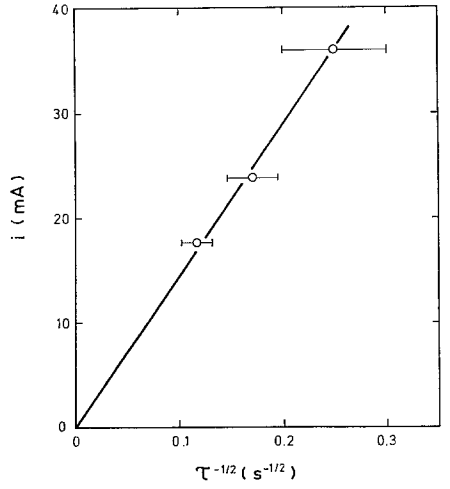

Fig. 4. Current vs $\tau^{-1/2}$ for low drain cells (11.6 X 2.1 mm, manufacturer A). Average values of 10 samples measured at three currents. A recovery time of at least 2 days was observed between each measurement. The average charge removed was 1.56% C_{nom} per cell for three measurements; average $i\tau^{1/2} = 145$ mA $s^{1/2}$.

For a given undischarged cell the dependence of the transition time on the current level followed the Sand equation, at least in the 10 to 200 s range of τ (see Fig. 4). The charge removed in the three measurements of Fig. 4 was 0.75 mA h or 1.6% of the nominal capacity per cell. The use of a lower current level, i.e. a longer transition time, would increase significantly the charge removed in the experiment and might, in addition, introduce the effect of convection. The results of Fig. 4 correspond to the normal semi-finite linear diffusion on a planar electrode and not to the typical behaviour of a thin layer cell for which a $i\tau =$ constant relationship should be observed.

Typical dependences of the passivation time constant $i\tau^{1/2}$, on the state-of-discharge are shown in Fig. 5 for the same cells as in Figs. 1 and 2. A nearly linear decrease of $i\tau^{1/2}$ vs state-of-discharge was usually observed between about 40 and 100% state-of-discharge. The slope of the $i\tau^{1/2}$ vs state-of-discharge curve between 0 and about 40% state-of-discharge changed significantly from one type of cell to the other: negative and positive slopes were observed for both low and high drain cells. Fig. 5 gives the typical behaviour for the same cells as in Figs. 1 and 2. Usually, for a given size, the passivation time is longer for a high drain cell (KOH) than for a low drain cell

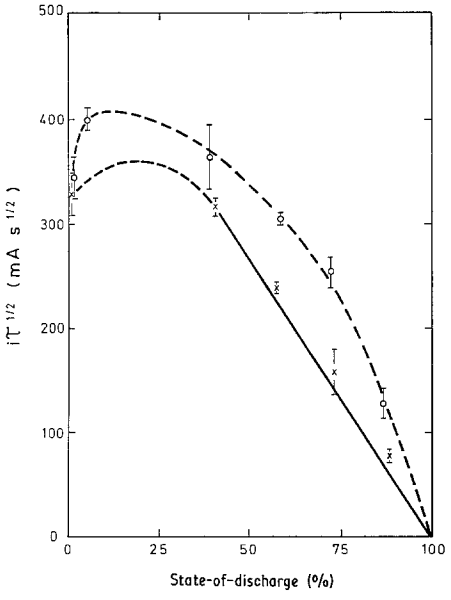

Fig. 5. Passivation time constant vs state-of-discharge for the same cells as in Figs. 1 and 2. Average values of five samples at each state-of-discharge. Low drain (X), high drain (○).

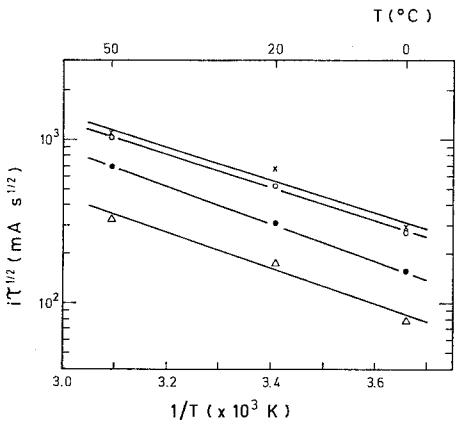

Fig. 6. Temperature dependence of $i\tau^{1/2}$ for low drain cells (11.6 × 3.6 mm, manufacturer A). Average values of five samples at each state-of-discharge. A recovery time of at least 2 days was observed between each measurement. A current of 15, 50 and 70 mA was used at 0, 20 and 50° C, respectively. The measurements were performed at 0 (○), 40 (X), 75 (●) and 90% (△) state-of-discharge.

(NaOH). To that respect the example shown in Fig. 5 is not representative of the general trend.

The variation of the passivation time constant with the state-of-discharge could be used as a state-of-discharge indicator. This method would, however, present two main drawbacks as compared to the technique proposed below, namely, (a) the charge removed during the measurement is not negligibly small due to the large value of either i or τ and (b) a long recovery time is required before normal behaviour is obtained after polarization of the cell into the diffusion domain. In addition, it should be mentioned that a passivation time $\leqslant$ 30–40 s for the undischarged cell would require a test current twice as large as in the method which will be proposed below. For most of the cells it will mean an ohmic drop larger than the cell potential. Also, for most of the cells, the bell shape variation of $i\tau^{1/2}$ in the low state-of-discharge range precludes the determination of the state-of-discharge at values $\leqslant$ 40%.

In order to check any significant change of behaviour with temperature, the passivation time was also measured as a function of the temperature at several states-of-discharge. A typical variation of $i\tau^{1/2}$ as a function of reciprocal temperature is shown in Fig. 6. An activation energy of 0.20–0.22 eV was found between 0 and 50° C, independently of the state-of-discharge. Such a value is typical for a diffusion-controlled process. The lack of variation of the activation energy with the state-of-discharge precludes the use of the variation of a diffusion-related parameter with temperature as a good state-of-discharge indicator.

Considering again the galvanostatic curves of Figs. 1 and 2, the potential at a given time, e.g. 10 or 30 s, could be used as state-of-discharge indicator instead of the passivation time. Typical plots of the potential after 10 s as a function of the state-of-discharge are shown in Figs. 7 and 8. A sloping decrease of the potential vs state-of-discharge was found, with significant variations from one type of cell to the other, and, most of the time, a large scatter from one cell to the other in the same lot number. The scatter was partly due to the difference of the internal resistance, R, and, to a lesser extent, of the actual capacity. The correction for the ohmic drop could be made provided that R was determined independently for each sample at each state-of-discharge. Figs. 7 and 8 give examples of the effect of the correction of the ohmic drop on the values of the potential after 10 s. In the example of Fig. 7, the internal resistance increases with state-of-discharge; the slope of the corrected

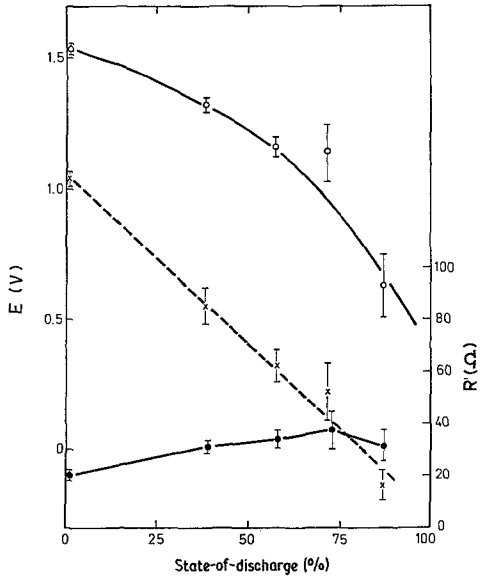

Fig. 7. Potential of the galvanostatic curve after 10 s vs the state-of-discharge for the same cells as in Fig. 1. Average value of five samples at each state-of-discharge $i = 25$ mA, potential after 10 s (X), potential after 10 s corrected for the ohmic drop RI (○), and internal resistance R (●).

potential vs state-of-discharge is therefore smaller than for the uncorrected potential. Fig. 8 shows the opposite example in which the slope of the corrected potential increases with respect to the uncorrected value because of a decrease of the

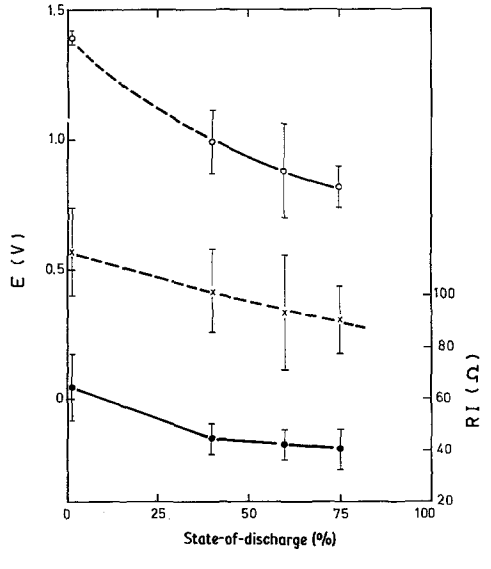

Fig. 8. Same as Fig. 7 for 7.9 × 2.1 mm (manufacturer C) low drain cells at $i = 12.5$ mA.

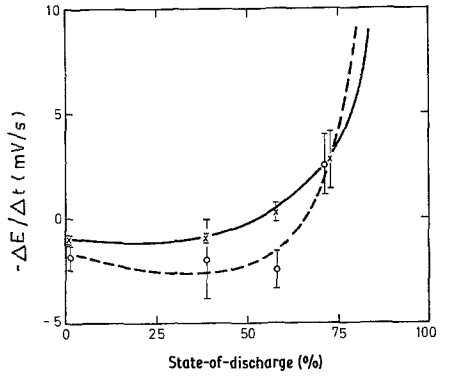

Fig. 9. $\Delta E/\Delta t$ between 2 and 10 s (○) and 10 and 30 s (X) vs state-of-discharge for the same cells as in Fig. 1, average values of five samples at each state-of-discharge, $i = 25$ mA.

internal resistance with state-of-discharge. In the latter case the scatter in the potential values decreases after correction for the ohmic contribution.

The values of the potential at a given time corrected or uncorrected for the ohmic drop are good candidates for a reliable state-of-discharge indicator. In the example of Fig. 7, an uncorrected potential after 10 s $\geqslant 0.6$ V would correspond to a state-of-discharge $\leqslant 40\%$. This method requires measurements in two different time domains, i.e. in the ms range for the determination of the ohmic drop and in the 10 s range for that of the potential.

Another way to correct for the ohmic contribution is to take the slope of the E vs t curve at a given time. Alternatively, the difference of potential between two appropriate times, $\Delta E/\Delta t$, could be measured. This value gives an average slope between two times. For the construction of a simple battery tester the latter value is simpler to measure than the slope at a given time. For this practical reason the $\Delta E/\Delta t$ value was investigated. The typical behaviour obtained for the same cells as in Figs. 1 and 2 are shown in Figs. 9 and 10. The time interval was usually chosen between 10 and 30 s. The $\Delta E/\Delta t$ value increased with increasing state-of-discharge and diverged to infinity at a given state-of-discharge. The latter sharp threshold might be taken as a state-of-discharge indicator. In the example of Fig. 10, a $\Delta E/\Delta t$ value of $\leqslant 15$ mV s^{-1} would correspond to a state-of-discharge $\leqslant 60 \pm 10\%$. For some cells

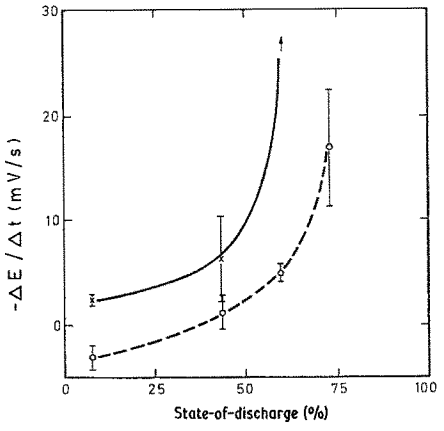

Fig. 10. Same as Fig. 9 for the same cells as in Fig. 2, i = 56 mA.

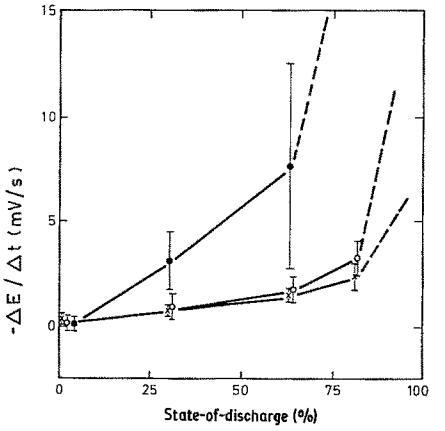

Fig. 12. Effect of the current on the $\Delta E/\Delta t$ value between 10 and 30 s for low drain cells (6.8 X 2.1 mm, manufacturer A), at i = 1.5 (X), 3.0 (○) and 4.5 (●) mA. Average values of five samples at each state-of-discharge.

the threshold occurred at a larger state-of-discharge as shown in Fig. 11. In the latter case the selection cannot be made at a state-of-discharge < 80% which is too large a value to be of practical use.

The threshold might be shifted to lower state-of-discharge values in two ways. The first one is to change the Δt at which $\Delta E/\Delta t$ is measured. Fig. 11 gives an example of a type of cell for which the threshold of the $\Delta E/\Delta t$ vs state-of-discharge could be shifted towards lower state-of-discharge values by measuring $\Delta E/\Delta t$ between 2 and 10 s instead of the more usual 10 and 30 s. In fact the $\Delta E/\Delta t$ vs state-of-discharge curve between 2 and 10 s of Fig. 11 does not show a true threshold but a nearly linear dependence

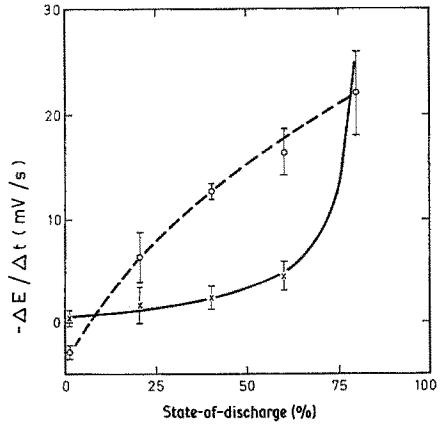

Fig. 11. Same as Fig. 9 for 9.5 X 1.6 mm (manufacturer A) low drain cells at i = 10 mA.

which can also be used to determine the state-of-discharge. For other types of cells this procedure did not produce any significant improvement (Fig. 9) or even shifted the threshold towards the higher state-of-discharge values (Fig. 10). The second way is to increase the level of the current.

An example of the influence of the level of current on the $\Delta E/\Delta t$ vs state-of-discharge curves is shown in Fig. 12. At a given state-of-discharge the absolute value of $\Delta E/\Delta t$ increased sharply with increasing current (Fig. 12). The change of $\Delta E/\Delta t$ was not a linear function of the level of the current. The variation of this parameter as a function of state-of-discharge was usually too small at low current levels to be used as a state-of-discharge indicator. As the level of current increased the state-of-discharge threshold at which $\Delta E/\Delta t$ diverged was shifted towards the lower values of the state-of-discharge. It is also worth pointing out that, at a given state-of-discharge, the scatter from one cell to the other increased significantly with increasing current. Thus an increase of the level of current will usually result in lowering the state-of-discharge threshold at which the selection can be made. For a very limited number of cell types, however, both the increase of current and the change of Δt at which $\Delta E/\Delta t$ was measured were unsuccessful in decreasing the state-of-discharge threshold towards values lower than 80%.

The selection of the appropriate current to be used for the test required a calibration measure-

Table 2. Slope of the $i\tau^{1/2}$ vs C_{nom} and test current vs nominal capacity curves for the low drain cells investigated

Manufacturer	*Year of fabrication*	$i\tau^{1/2}/C_{nom}$ *(mA s$^{1/2}$/mA h)*	*Number of lots*	i_{mes}/C_{nom} *(mA/mA h)*	*Number of lots*
A	1980–1983	–*	37	–*	29
	1981	4.9	4	0.40	4
	1982	5.7	15	0.48	11
	1983	4.3	10	0.49	8
B	1982	6.5	10	0.51	9
C	1982	7.5	8	0.53	7
D	1982	8.2	6	0.69	5
E	1982	13.3	4	1.19	3
F	1983	–	–	0.34	3

* Highly dispersed

ment. A correlation between the test current and some characteristics of the cell would be very helpful in selecting the appropriate current for each type of cell. A correlation was found between the passivation time constant and the capacity of the cell. As expected, different slopes for low and high drain cells were noted. The slopes also varied for each manufacturer. Fig. 13 gives the correlation between $i\tau^{1/2}$ and C_{nom} for some low drain cells from three manufacturers. Table 2 gives the slope of the $i\tau^{1/2}$ vs C_{nom} curve for low drain cells of each manufacturer studied. The number of high drain cells investigated was too small to give a reasonable correlation.

For low drain cells from manufacturers A–D the following rough correlation was found:

$$i\tau^{1/2}(\text{mA s}^{1/2}) \simeq 6\, C_{nom}\ (\text{mA h}) \qquad (1)$$

As the current level was chosen in order to have a passivation time of about 150 s for the undischarged cells, the following correlation should hold between the current and the nominal capacity:

$$i_{test}\ (\text{mA}) \simeq 0.5\, C_{nom}\ (\text{mA h}) \qquad (2)$$

This has indeed been found for the current giving a $\Delta E/\Delta t$ response from which the selection criteria was $\leqslant 60\%$ state-of-discharge (see Fig. 14 and Table 2).

In the correlations (Equations 1 and 2) the cell capacity was used as a parameter instead of the volume because the former is a more often used characteristic of a cell. Obviously the correlation would also hold for both anode and cell volumes.

Over a period of three years, the passivation time constant was found to change as a function

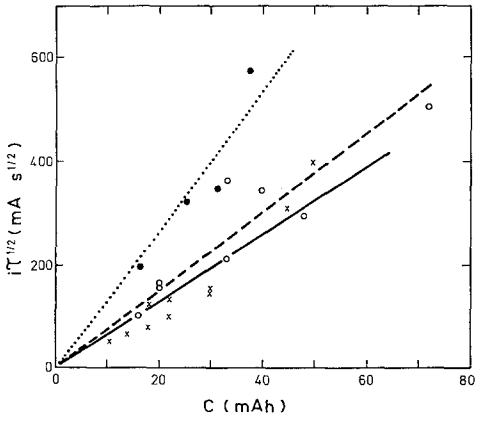

Fig. 13. Passivation time constant vs nominal capacity for some low drain cells of manufacturers B (×), C (○) and E (●).

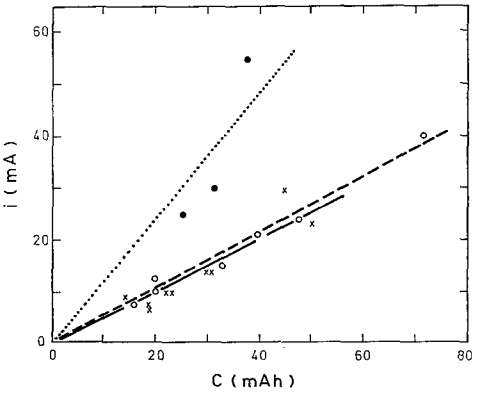

Fig. 14. Test current vs nominal capacity for some low drain cells of manufacturers B (×), C (○) and E (●).

of the date of fabrication for the same type of cell from the same manufacturer. In the extreme case the passivation time constant decreased from 230 down to 60 mA $s^{1/2}$. This behaviour will constitute a limitation for the determination of the state-of-discharge without calibration for each lot number.

Finally, some idea of the dispersion obtained in a blind test would be helpful. Such a test was made with the assistance of an outside laboratory in which the initial discharges were made to some state-of-discharge unknown to us. One hundred low drain cells (7.9 × 2.1 mm, manufacturer F), from one lot number were used. Approximately one third was discharged for 31, 52 and 74%, respectively, of their nominal capacity. The cells were then sent to us for the state-of-discharge test. From earlier measurements carried out on 25 cells from the same manufacturer but not necessarily from the same lot a current level of 15 mA was known to be appropriate for selecting the cells at $> 50 \pm 10\%$ with a $\Delta E/\Delta t$ value < 5 mV s^{-1} between 10 and 30 s. The cells were returned to the outside laboratory and discharged completely to determine the remaining capacity which was compared with the predicted state-of-discharge. The per cent of discharge, $\%\, D$, was calculated with respect to the mean capacity, $\bar{C}$, using the remaining capacity, C_r, as follows:

$$\%\, D = \frac{\bar{C} - C_r}{\bar{C}} = 1 - \frac{C_r}{\bar{C}} \qquad (3)$$

The plot $\Delta E/\Delta t$ vs effective state-of-dicharge is given in Fig. 15. The results indicate that only five cells fell outside the dispersion limit, i.e. 40–60% D. Four of these five cells were predicted to be good and found to be bad while only one was in the inverse situation. A success ratio of 93% may be calculated neglecting the cells with a capacity between 40 and 60% state-of-discharge. The levels of discharge, i.e. 23–77%, were very close to the dispersion limit of the method (40–60%). The test conditions were therefore particularly difficult as there was no fresh or nearly exhausted cell. The success ratio is expected to depend on the number of cells in each state-of-discharge. Despite these difficult conditions the success ratio was rather good. The 7% of wrong

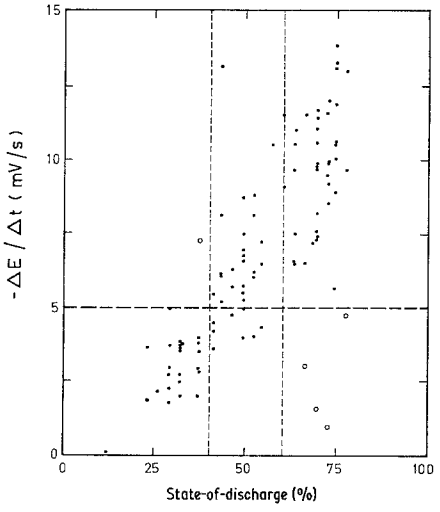

Fig. 15. $\Delta E/\Delta t$ between 10 and 30 s for 100 low drain cells (7.9 × 2.1 mm, manufacturer F) as a function of the state-of-discharge. One third of the cells were predischarged at 31, 52 and 74%, respectively of their nominal capacity. The results show that for only five samples out of 67 (○) the predicted state-of-discharge was wrong, neglecting results in the range 40–60% D.

predictions, excluding results in the 40–60% range, as mainly due to the dispersion of the electrical characteristics of the cells as shown in Fig. 15.

4. Discussion

4.1. *Electrode processes*

The processes which occur at the zinc and silver oxide electrodes have been investigated thoroughly and reviewed recently [6]. The overall reaction for the alkaline Zn/Ag_2O cell is:

$$Zn + Ag_2O \rightleftharpoons 2\,Ag + ZnO \qquad (4)$$

For the positive electrode the probable reaction sequence involves a dissolution–precipitation mechanism in which there is dissolution of Ag_2O

$$Ag_2O + 2\,OH^- + H_2O \rightleftharpoons 2\,Ag(OH)_2^- \qquad (5)$$

followed by migration of the dissolved species to an electronic conducting point in the positive mass where it is reduced to metallic silver [7]

$$Ag(OH)_2^- + e \rightarrow Ag + 2OH^- \qquad (6)$$

A parallel solid-state mechanism might also take place by migration of O^{2-} ions through the Ag_2O

phase. These ions are removed as OH^- ions by reaction with water.

The discharge of the zinc electrode produces a supersaturated zincate solution via the reaction

$$Zn + 4\ OH^- \rightarrow Zn(OH)_4^{2-} + 2e \qquad (7)$$

from which porous ZnO is precipitated on the electrode surface by the chemical reaction

$$Zn(OH)_4^{2-} \rightarrow ZnO + 2OH^- + H_2O \qquad (8)$$

The reasonable maximum estimate of the critical concentration of $Zn(OH)_4^{2-}$ above which ZnO precipitates is 3 molar [6, 8]. This value and the volume of the electrolyte lead to the conclusion that discharge without precipitation of ZnO (primary phase discharge) constitutes about 15% of the total capacity of a typical Zn–Ag_2O button cell. The occurrence of the precipitation of ZnO might explain the change of slope of the $i\tau^{1/2}$ vs state-of-discharge curve at state-of-discharge $\leqslant$ 40% (see Fig. 5).

When the rate of mass transfer of OH^- ions across the porous ZnO layer is below that for the reaction (7), the continuing discharge yields compact ZnO by the reaction

$$Zn + 2\ OH^- \rightarrow ZnO + H_2O + 2e \qquad (9)$$

which further limits the rate of mass transfer of OH^-. Passivation occurs when the ZnO film covers the whole zinc surface.

4.2. *Galvanostatic discharges*

Many workers [9] have made galvanostatic studies using planar zinc electrodes in alkaline solutions. There are conflicts as to whether the Sand equation can cover the entire current density region or two equations are required for high and low current density regions. Free convection usually complicated the interpretation of the results.

Experiments performed with button cells with a limited range of current densities (see Fig. 4) confirm earlier studies made using planar zinc electrodes. Convection is usually assumed absent at battery electrodes, although careful observations have revealed the presence of small convection currents even on horizontal planar electrodes [6]. Complication in the interpretation of the experimental data, therefore, is not expected to arise from the latter effect but mainly from the porous nature of the zinc electrode.

Elsdale *et al.* [10] found that the major source of passivation of a microporous zinc electrode was the formation of insoluble ZnO within the electrode pores. In their experiments the transition from the active to the passive electrode condition was not abrupt as is well established for a planar zinc electrode in alkali [11], rather a gradual increase in electrode potential was observed, corresponding to the electrode reaction being driven deeper into the anode as discharging pores became blocked with oxide. The shapes given in Figs. 1 and 2 are not typical of planar or of microporous electrodes but indicate a mixture of both geometries.

Short-time passivation behaviour on planar electrodes under quiescent conditions have been completely explained on the basis of semi-infinite diffusion theory and the onset of passivation at a critical $Zn(OH)_4^{2-}$ concentration at the charge transfer surface. The effective surface area, S, is needed to calculate the diffusion coefficient, D_O, from the Sand equation:

$$\tau^{1/2} = \frac{nFS\,D_O^{1/2}\,\pi^{1/2}C_O^*}{2i} \qquad (10)$$

From the results shown in Fig. 13, it is evident that the effective surface area changes not only with the apparent surface area but also with the volume of the cell. This result implies that the pore dimensions in the undischarged state are larger than the diffusion layer $\delta = 2\,(Dt/\pi)^{1/2} \simeq$ 0.3 mm for $D_O = 5 \times 10^{-6}$ cm^2 s^{-1} [12] and $t = 150$ s. This estimation of the thickness of the diffusion layer is roughly compatible with the zinc particle size comprised between 75 and 400 μm depending on the height of the cell. The effective surface area may be calculated from Equation 10 using the diffusion coefficient for zincate ions in 8N KOH, $D_O = 5 \times 10^{-6}$ cm^2 s^{-1} [12], the concentration of zincate ions in in saturated solution $C_O^* = 0.5$ mM cm^{-3} [12] and $n = 2$:

$$S = 5.23i\tau^{1/2}$$

with S in cm^2, i in A and τ in s.) (11)

The effective surface area calculated using Equa-

tion 11 varies between 0.13 cm^2 for the smaller cell investigated (i.e. a 6.8 x 1.1 mm cell, manufacturer A, apparent surface area: 0.13 cm^2, $i\tau^{1/2} = 25$ mA $s^{1/2}$) and 7.5 cm^2 for the larger cell measured (i.e. a 11.6 x 5.4 mm cell, manufacturer F, apparent surface area: 0.48 cm^2, $i\tau^{1/2} = 1420$ mA $s^{1/2}$). The value of S is strongly influenced by the value C_O^* used in the calculation. The value chosen gives reasonable results since the surface area corresponds roughly to the apparent area for the thinner cell investigated. This is understandable since the thickness of the thinnest zinc electrode is roughly that of the largest particle size of the zinc powder. An effective surface area two times larger would be calculated using a C_O^* value of 0.25 mM cm^{-3}, which would also be an acceptable bulk concentration for zincate.

The preceding results are in agreement with published data obtained with unamalgamated zinc powders for which the passivation time constant was found to increase with increasing average particle size of the zinc powder [13]. For a given geometry, the coarser the particle size, the larger the accessible electrode area and the larger the passivation time constant. The accessible area is that defined by the thicker diffusion layer (at the longer time). A ten-fold increase of passivation time in 10 N KOH has been reported between smooth and microporous (0.8 m^2 g^{-1} and 72% porosity) electrodes. These results are somewhat at variance with reports indicating that only a small part of the interior of a porous zinc electrode participates in the electrochemical process [14] and that the characteristic reaction penetration depths vary between 150 (initial value) to 80 μm (steady state) for a pore size of 265 μm and a porosity of 13% [15].

4.3. *Dependence of $i\tau^{1/2}$ on state-of-discharge*

The passivation time constant decreases with increasing state-of-discharge between 40 and 100% state-of-discharge. The variation between 0 and 40% state-of-discharge changed significantly from one type of cell to the other. It has already been pointed out that the initial change is most likely attributed to the occurrence of the primary phase discharge which takes place without precipitation of ZnO. The variation from one manufacturer to the other and from one type of cell to the other reflects changes in chemistry and construction. The nearly linear decrease of $i\tau^{1/2}$ above 40% state-of-discharge is most likely due to the decrease of the surface area, S, by precipitation of compact ZnO. In addition to passivation, conversion of Zn to ZnO during discharge decreases the pore size and thus limits the transport of electrolyte into the interior of the porous electrode. Pore plugging may explain the deviation from linearity sometimes observed in the $i\tau^{1/2}$ vs state-of-discharge plot in the 40–100% state-of-discharge range. The curved relationship between $i\tau^{1/2}$ and state-of-discharge below about 40% state-of-discharge is a serious and fundamental limitation to the use of this criterion as a state-of-discharge indicator at levels $\leqslant 40\%$.

4.4. *Slope of the galvanostatic discharge curve vs state-of-discharge*

Except for the measurements performed with a reference electrode (Fig. 3) the galvanostatic curves reported in the present paper were recorded using the cell potential. Under these experimental conditions it is difficult to determine whether the wave is totally reversible (Nernstian behaviour), partly reversible or totally irreversible. The slope of the E vs t curve differs according to the reversibility of the process [16]. However, the following calculations will show that the main changes of the slope vs time of discharge are not very different for reversible and irreversible waves.

In constant current electrolysis the potential is given by the following equation for reversible waves [16]:

$$E = E_{\tau/4} + \frac{RT}{nF} \ln \frac{\tau^{1/2} - t^{1/2}}{t^{1/2}} \qquad (12)$$

with

$$E_{\tau/4} = E^{0\prime} - \frac{RT}{2nF} \ln \frac{D_O}{D_R} \qquad (13)$$

and

$$\tau^{1/2} = \frac{nFs}{2i} D_O^{1/2} \pi^{1/2} C_O^* = \frac{A}{i} \qquad (14)$$

with

$$A = \frac{nFs}{2} D_O^{1/2} \pi^{1/2} C_O^* = i\tau^{1/2} \qquad (15)$$

in which $E_{\tau/4}$ is the potential where $i/id = 1/4$, $E^{0\prime}$ is the formal potential, R is the gas constant, T is the absolute temperature, n is the number of faradays per mole, D_O and D_R are the diffusion coefficients of the oxidized and reduced species, S is the area and C_O^* is the initial concentration of species O.

The slope of the E vs t curve can be calculated as

$$\frac{dE}{dt} = -\frac{RT}{2nFt}\,\frac{1}{(1-it^{1/2}/A)} \qquad (16)$$

For totally irreversible waves the potential is given by [16]:

$$E = E^{0\prime} + \left(\frac{RT}{\alpha n_a F}\right) \ln\left[\frac{2k^0}{(\pi D_O)^{1/2}}\right] + \left(\frac{RT}{\alpha n_a F}\right) \ln(\tau^{1/2} - t^{1/2}) \qquad (17)$$

with α being the transfer coefficient, n_a the number of electrons involved in the rate determining step and k^0 the standard heterogeneous rate constant, and the slope of the E vs t curve is calculated as:

$$\frac{dE}{dt} = -\frac{RT}{2\alpha n_a F}\,\frac{1}{[t^{1/2}(A/i - t^{1/2})]} \qquad (18)$$

For both reversible and irreversible waves the slope is always negative with a maximum at $t/\tau = 4/9$ and $1/4$, respectively. It varies relatively little in the vicinity of the inflexion point.

The slope of the E vs t curve depends on i, t and A (see Equations 16 and 18). It is of interest to calculate the variation of the slope as a function of the state-of-discharge using the nearly linear relationship found between A and D (see Fig. 5)

$$A = A_0\,(1-D) \qquad \text{for } 0 < D < 1 \qquad (19)$$

with A_0 representing the value of A at $D = 0$. Substituting Equation 19 into Equation 16 the slope of the E vs t curve for a reversible wave is given by

$$\frac{dE}{dt} = -\frac{RT}{2nFt}\,\frac{1}{1 - it^{1/2}/A_0(1-D)} \qquad (20)$$

Similarly for an irreversible wave the slope as a function of D is found by substituting Equation 19 into Equation 18:

$$\frac{dE}{dt} = -\frac{RT}{2\alpha n_a F}\,\frac{1}{t^{1/2}[A_0(1-D)/i - \tau^{1/2}]} \qquad (21)$$

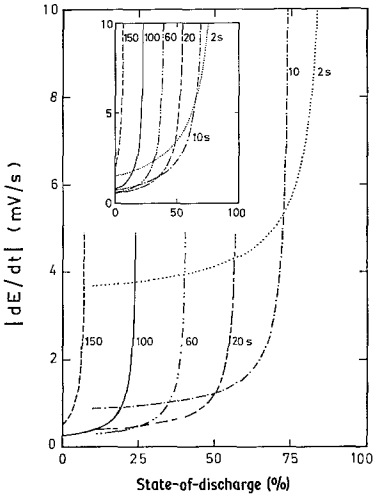

Fig. 16. Slope $|dE/dt|$ as a function of the state-of-discharge calculated for a reversible wave according to Equation 20 at six different times for $n = 2$, $A_0 = 400$ mA $s^{1/2}$ and $i = 30$ mA. The insert shows the same curves for an irreversible wave according to Equation 21 with $\alpha = 0.5$ and $n_a = 1$.

Fig. 16 gives the absolute value of the slope, $|dE/dt|$, calculated at six different fixed times as a function of the state-of-difference for a given i and A_0 for reversible and irreversible waves. The slope at a given time and A_0 is given in Fig. 17 for six different values of i. The slope diverges to infinity for a limiting value D^* given

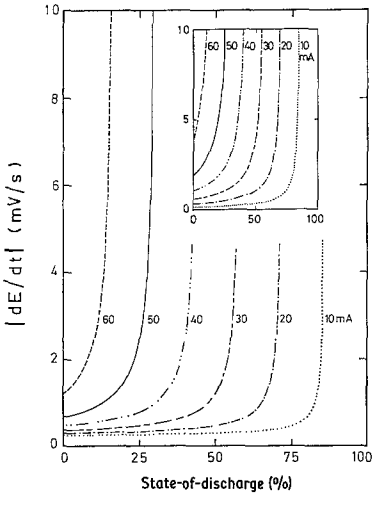

Fig. 17. Slope $|dE/dt|$ as a function of the state-of-discharge calculated for a reversible wave according to Equation 20 at six different currents for $n = 2$, $A_0 = 400$ mA $s^{1/2}$ and $t = 30$ s. The insert shows the same curves for an irreversible wave according to Equation 21 with $\alpha = 0.5$ and $n_a = 1$.

by:

$$D^* = 1 - it^{1/2}/A_0 \qquad (22)$$

for both reversible and irreversible waves. For a given A_0, D^* is higher, the lower the values of time, t, and current, i. This limitation reflects the fact that both Equations 20 and 21 are restricted to the range $t < \tau$.

It is worth pointing out that the linearity of curve A vs state-of-discharge is usually observed only for $40 < D < 100\%$. A more precise calculation of the slope vs state-of-discharge could have been done in the 0–40% state-of-discharge range. A value of $i\tau^{1/2}$ smaller than that predicted by the linear relationship between $i\tau^{1/2} = A$ and the state-of-discharge (see Equation 19) observed between 0 and 40% state-of-discharge (see Fig. 5) would correspond to a slope larger than that calculated using Equations 20 or 21. This behaviour would explain the dip in the $\Delta E/\Delta t$ state-of-discharge curve sometimes found in the low state-of-discharge range (see Fig. 9).

Figs. 16 and 17 show that at low values of t and i, it will only be possible to select the cells at a high value of the state-of-discharge, say 80%. On the contrary, a long time, a high current or both, are required to select the cells at a small state-of-discharge. In practice, this is unfortunate since the time and current should be as small as possible to limit the time of measurement and the charged extracted. A trade-off therefore has to be made between the critical value of the state-of-discharge, D^*, the time, t, and the current, i. In the present investigation the current has been chosen to have a selection at 50 ± 10% state-of-discharge using a time $\leqslant 30$ s.

4.5. *Characteristics of the method of state-of-discharge determination*

The proposed state-of-discharge indicator for zinc–silver oxide button cells is based on the measurement of the $\Delta E/\Delta t$ value at two times smaller than 30 s. Applications are limited to a 'go/no go' test. In the following the ideal requirements for such a determination will be compared with what is achievable.

1. The selection should be made at a state-of-discharge $\leqslant 30\%$ (i.e. $\geqslant 70\%$ of the fully-charged state). The nonlinear relationship found for most of the cells between $i\tau^{1/2}$ and the state-of-discharge in the 0–40% range prevents a selection at values of $\leqslant 40\%$ state-of-discharge.
2. The charge withdrawn during the measurement should be as small as possible. Typical values are in the 0.1% range.
3. The time required for the measurement should be as short as possible. A time of 10 or 30 s is used.
4. The selection parameter should be independent of the parameter of the measurement. The current level influences the slope or $\Delta E/\Delta t$ value. An appropriate current level should therefore be used to achieve a given $\Delta E/\Delta t$.
5. The selection and measuring parameters should be independent of the dimensions and of the manufacturer of the cell. A calibration is necessary for each cell dimension, and, possibly, for each manufacturer. A rough correlation between the current level and the cell capacity helps in selecting the appropriate test current.
6. The response should be independent of the history of the cell. This parameter has not been systematically investigated.
7. The principle of the method should be as simple as possible to permit the fabrication of a low cost tester. This is indeed the case and a simple device has been built which measures the cells at an appropriate current for 30 s and predicts if the state-of-discharge is more or less than 50% of the nominal capacity.

The main drawbacks of the method are as follows:

(a) the need for a calibration for each lot of cells,

(b) the lack of universality. Eleven types of cell out of 96 investigated could not be selected successfully, mainly because of (i) too large a dispersion of the electrical characteristics of the cells, occurring especially for small, newly developed types, and (ii) state-of-discharge value at which selection was possible was too high to be of practical use.

The threshold value of $\Delta E/\Delta t$ at which the selection was made was usually chosen to be severe

which implies the elimination of more good cells than the retention of defective ones. In this context it may be pointed out that the galvanostatic method uses current levels orders of magnitude larger than the normal average discharge current. Under the test conditions, only the surface area in good ionic contact takes part in the electrode reactions, while, under the normal discharge conditions, a larger surface area and volume might contribute to the total capacity by slow diffusion processes. This may explain why cells predicted to be bad were more often found to be good than the inverse. (In this respect the results shown in Fig. 15 are not representative of the typical case).

Finally, the proposed method does not predict a cell failure due to an internal short-circuit occurring after the test.

Acknowledgements

The author is pleased to thank F. Züllig for his skillful assistance in the experimental work and in the analysis of the data, R. Jeanmonod for designing and building a simple tester, R. Viennet for assistance in the mathematical analysis and A. Hoffmann for helpful discussions in the early stage of this work.

References

[1] F. Kornfeil, *J. Electrochem. Soc.* **123** (1976) 1271.
[2] S. Lerner, H. Lennon and H. N. Seiger, in 'Power Sources 3' (edited by D. H. Collins) Oriel Press, Newcastle upon Tyne (1971) p. 135–148.
[3] S. Sathyanarayana, S. Venugopalan and M. L. Gopikanth, *J. Appl. Electrochem.* **9** (1979) 125.
[4] J. J. Winter, J. T. Breslin, R. L. Ross, H. A. Leupold and F. Rothwarf, *J. Electrochem. Soc.* **122** (1975) 1434.
[5] J. -P. Randin, *J. Appl. Electrochem.* **15** (1984).
[6] F. L. Tye, in 'Electrochemical Power Sources' (edited by M. Barak) Peter Peregrinus for the IEE, London (1980) p. 50–150.
[7] T. D. Dirkse, D. DeWit and R. Shoemaker, *J. Electrochem. Soc.* **114** (1967) 1196.
[8] M. B. Liu, G. M. Cook and N. P. Yao, *ibid.* **129 (1982) 1390.**
[9] *Idem, ibid.* **128** (1981) 1663 and references therein.
[10] R. N. Elsdale, N. A. Hampson, P. C. Jones and A. N. Strachan, *J. Appl. Electrochem.* **1** (1971) 213.
[11] Y. Sato, H. Niki and T. Takamura, *J. Electrochem. Soc.* **118** (1971) 1269.
[12] T. P. Dirkse, in 'Power Sources 3' (edited by D. H. Collins) Oriel Press, Newcastle upon Tyne (1971) p. 485–493.
[13] G. Coates, N. A. Hampson, A. Marshall and D. F. Porter, *J. Appl. Electrochem.* **4** (1974) 75.
[14] M. W. Breiter, *Electrochim. Acta* **15** (1970) 1297.
[15] M. B. Liu, G. M. Cook, and N. P. Yao, *J. Electrochem. Soc.* **129** (1982) 239.
[16] A. J. Bard and L. R. Faulkner, 'Electrochemical Methods, Fundamentals and Applications', J. Wiley, New York (1980) p. 256–258.

Publisher's note

Part II will appear in the next issue.